Journal of New Technology and Materials (JNTM)
J. New Technol. Mater.
Vol. 10, N°01 (2020)31-37

OEB Univ. Publish. Co.

Synthesis and characterization of Fe_3O_4–MWCNTs adsorbent: application for bromocresol purple dye removal in aqueous medium

Zehoua Rehimi[a], Hassan Ayadi[b] and Sabrina Halladja[a,c]

[a] *Laboratory of Anticorrosion-Materials, Environment and Structures, Faculty of Technology, University of 20 Août 1955, Skikda 21000, Algeria*
[b] *Laboratory of Physico-Chemistry Research of Surfaces and Interfaces, Faculty of Sciences, University of 20 Août 1955, Skikda 21000, Algeria*
[c] *Laboratory of Innovative Techniques for the Environment Preservation, Faculty of Exact Sciences, University of Mentouri, Constantine 25000, Algeria*

Corresponding author, email: z.rehimi@univ-skikda.dz

Received date: Oct. 31, 2019 ; revised date: Feb. 24, 2020 ; accepted date: Apr. 24, 2020

Abstract

Magnetic nanocomposite was synthesized from iron salts and multi-walled carbon nanotubes (Fe_3O_4–MWCNTs) using the chemical coprecipitation method. The characterization of Fe_3O_4–MWCNTs adsorbent was carried out using X-Ray diffraction (XRD); Fourier transform infrared spectroscopy (FTIR); Brunauer-Emmett-Teller (BET) and scanning electron microscopy (SEM). The prepared material has exhibited a higher adsorption capacity 296.52 mg.g^{-1} to remove the Bromocresol purple (BCP) dye from aqueous solutions. Kinetic study shows that the equilibrium time reached after 80 minutes and the pseudo second order best suited this adsorption. Isotherm models indicate that the adsorption represented perfectly by the Langmuir. Thermodynamic study suggests that the sorption process is spontaneous, exothermic and physisorption type. This work focused on the efficiency of nanocomposite Fe_3O_4–MWCNTs as a magnetically separable adsorbent compared with pure multi-walled carbon nanotubes.

Keywords: Carbon nanotubes; magnetite; composite; dye; adsorption.

1. Introduction

Aquatic pollution is one of the most serious issues facing the humanity today, several contaminants like heavy metals [1], metalloids, pesticides and dyes invaded wastewater and caused health hazards [2]. About 7×10^5 tons / year of pigments and dyes are synthesized [3], and used in many fields like industrials, cosmetic, pharmaceutical, painting, textile and food [4]. Dyes whatever acidic or basic can be carcinogenic, mutagenic and toxic due to their complex aromatic structures, stability to biological degradation, and persistent nature in effluents [3,5]. Bromocresol purple is one of the organic dyes that can be produced from textile, paper, industries and pharmaceutical. Consequently, the disposal of such product could be harmful to the environment and human health by causing several diseases [6]. Nowadays, the removal of dyes in aqueous medium captivates the interest of many researchers around the world. Various methods are using in water remediation like conventional techniques which become not efficient enough for recalcitrant contaminants [7], adsorption [8], extraction [6], advanced oxidation processes [9], ozonation and photocatalysis, etc [10]. Only few studies have focused on the removal of Bromocresol Purple [6]. As reported by Farida M. S. E. El-Dars et al , the adsorption of BCP was carried out by using bentonite carbon composite at high temperature T= 313 K, the maximum adsorption capacity estimated to (Q_{max} = 0.1463 mg.g^{-1}) and equilibrium time achieved in 60 minutes [11]. Photochemical degradation of BCP dye was investigated also by Bousnoubra et al [12]; the present work studies the adsorption of BCP using a nanocomposite of commercial (MWCNTs) modified with magnetite (Fe_3O_4). The multi-walled carbon nanotubes adsorbent have an outstanding performance could be ascribed to its high adsorption capacity, unique structure, chemical stability [13] and huge specific surface area, etc [14]. Until now, the use of MWCNTs as adsorbent for BCP removal is very scarce in literature. To improve the performance of the dye removal by MWCNTs, magnetite lends support and enhances the adsorption process by faster and easier separation compared with boring filtration or centrifugation; the Fe_3O_4 may contribute as well in the adsorption process for dye removal [15]. In this context the Fe_3O_4–MWCNTs adsorbent was prepared using the coprecipitation method and characterized by X-ray diffraction, Fourier transform infrared spectroscopy, the Brunauer-Emmett-Teller and scanning electron microscopy analysis. Kinetics and equilibrium experiments of BCP dye adsorption onto the synthesized adsorbent studied in batch system.

2. Experimental

2.1. Materials

MWCNTs (Nanocyl 7000, diameter 1−10 nm, length 60−100 nm, purity >90%) were purchased from Nanocyl. Nitric acid 53% were purchased from Montplet & Esteban SA. Sodium was purchased from Prolabo (purity 98%); Hydrochloric acid was purchased from Sigma Aldrich. Ferrous sulfate heptahydrate ($FeSO_4.7H_2O$), ferric chloride hexahydrate ($FeCl_3.6H_2O$) and Bromocresol purple BCP dye were purchased from Biochem, these reagents were used without further purifications, all aqueous solutions were prepared using distilled water. The spectrophotometric measurements were performed with UV-visible Shimadzu 1605; X-ray Diffractometer system XPERT-PRO was utilized to identify the existing phases in nanocomposite. Analysis morphological examination of the nanocomposite was carried out by scanning electron microscopy (SEM) (model DSM 962; Carl Zeiss Meditec AG, Jena, Germany) ; Fourier Bruker infrared microscope "Hyperion 2000" This equipment is coupled with a Vertex 70 interferometer and optimized for Mid-IR (4000-400 cm^{-1}); specific surface area was obtained through a micromeritics ASAP- 2020.

2.2. Samples preparation

To improve the adsorption efficiency of the MWCNTs, it is necessary that an oxidation step be performed to purify, open and cut extremities; in order to facilitate their functioalization to their composites by the enhancement of interfacial adhesion [16]. The most common method is to add carboxylic acid groups onto the surface of MWCNTs by chemical oxidation using nitric acid [17]. Therefore, a small amount equal to 1g of MWCNTs was oxidized by 200 mL of HNO_3 (3M) then sonicated for 1 h to disperse the sample very well in the solution. After that at 100°C the mixture was stirred for 4 h then it was rinsed and filtrated with distilled water until the filtrate became neuter, the obtained material was dried at 80°C and calcined at 450 °C for 4h. The modification of oxidized MWCNTs by magnetite was occurred by coprecipitation method; in 75 mL of mixture containing 1.49 g $FeCl_3.6H_2O$ and 0.76g $FeSO_4.H_2O$; 0.5g of oxidized carbon nanotubes were added into the solution and stirred at 70°C under inert gas N_2. The precipitation of Fe_3O_4 required basic medium so, 15 ml of NaOH (0.5 M) was added by dropwise until pH=11. The mixture was stirred and heated at 70°C for 3 h to realize the following reaction:

$$Fe^{2+}+2Fe^{3+}+8OH^-+MWCNTs \rightarrow Fe_3O_4-MWCNTs+4H_2O$$

The nanocomposite obtained was washed several times and dried at 100°C for 4 h [15]. The magnetite was prepared using the coprecipitation method as described by Poedji Loekitowati Hariani et al [18].

2.3. Adsorption process

The Fe_3O_4−MWCNTs nanocomposite (20 mg) was added to 200 mL of BCP (10 $mg.L^{-1}$). The mixture was stirred at intervals of time ranging from 1 min to 120 min. After that, the residual dye concentration was determined by spectrophotometer using suitable calibration curves at appropriate wavelengths corresponding to λ_{max} = 431 nm the maximum absorbance. A simple separation was carried out using the permanent magnet (fig. 1). The amount of dye adsorbed per unit of mass has been calculated using the following formula [19].

$$Q_t = \frac{(C_0 - C_t)V}{m} \quad (1)$$

Q_t: Adsorption capacity given by ($mg.g^{-1}$).
C_0: The initial concentration of dye ($mg.L^{-1}$).
C_t: The residual concentration of dye ($mg.L^{-1}$).
V: The volume of the solution (L).
m: The mass of the adsorbent used (g).

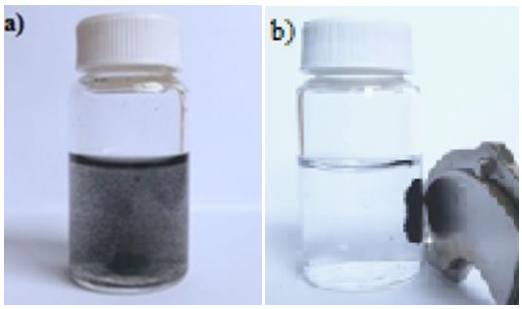

Figure1. (a). Before magnetic separation (b). After magnetic separation.

3. Results

3.1. Characterization of samples

The XRD patterns of both commercial MWCNTs (red color) and nanocomposite (black color) are represented in (fig. 2). The peaks At 2θ values about 26° indicate the presence of carbon nanotubes before and after modification, the presence of magnetite in the Fe_3O_4−MWCNTs spectra is confirmed by the appearing of new peaks at different 2θ values 30.1°, 35.5°, 43.1°, 53.5°, 57.0° and 62° [20]. To estimate the average size of the Fe_3O_4−MWCNTs composite, Debyee Scherrer formula was applied [21]:

$$D = \frac{0.9\lambda}{\beta cos\theta} \quad (2)$$

Where β (rad): The full width at half maximum (FWHM) of the diffraction; θ (rad): The Bragg's diffraction angle and λ=1.54060 A^0 the X-Ray wavelength of the copper (Cu) radiation used in XRD. The size of particles was found to be about 19±1 nm. The MWCNTs, Fe_3O_4 and Fe_3O_4− MWCNTs were analyzed by FTIR. As shown in (fig. 3), the peak at 580 cm^{-1} in both Fe_3O_4− MWCNTs and Fe_3O_4 curves is attributed to Fe−O bond; while 3398 cm^{-1} is referred to O-H in the magnetite and the nanocomposite. In the Fe_3O_4−MWCNTs pattern new peaks are slightly appear at 1393 cm^{-1} and 1587 cm^{-1} which

are indicated the presence of COO-Fe bond [22], 1651 cm^{-1} is referred to C=O stretching. The peak at 3450 cm^{-1} is appropriated to O-H stretching [15]. Surface Area analysis of Fe_3O_4– MWCNTs was carried out using the BET technique; (fig. 4) represents the isotherms of adsorption/desorption of N_2 onto Fe_3O_4 and Fe_3O_4–MWCNTs nanoparticles, these last are of type II. The isotherm of the Fe_3O_4 is less than that of nanocomposite indicates a lower specific surface area and lower adsorption quantity due to the porosity and high adsorbability of oxidized–MWCNTs [23]; the (Table 1) reveals some textural properties of the corresponding samples Fe_3O_4 and Fe_3O_4–MWCNTs. The SEM screened in (fig.5) the morphology of MWCNTs, Fe_3O_4 and Fe_3O_4–MWCNTs in images A, B and C, respectively. A homogenous surface of curly hair-like structure was shown in (image A) [24]; large quantities of spherical-shaped magnetite were observed in (image B) which were almost coated homogenously the multi-walled carbon nanotubes in the (image C) and the surface was relatively uniform.

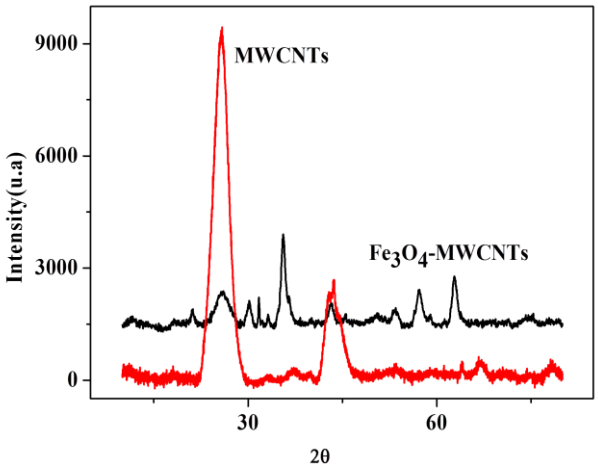

Figure 2. XRD patterns of MWCNTs and Fe_3O_4–MWCNTs

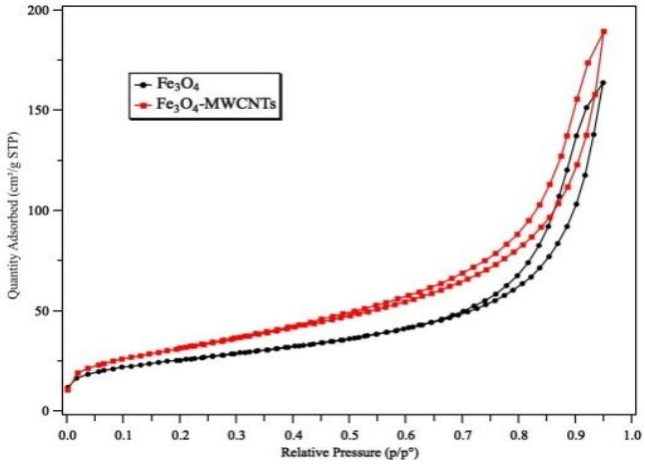

Figure 4. Nitrogen adsorption/desorption isotherm of the Fe_3O_4 and Fe_3O_4–MWCNTs samples

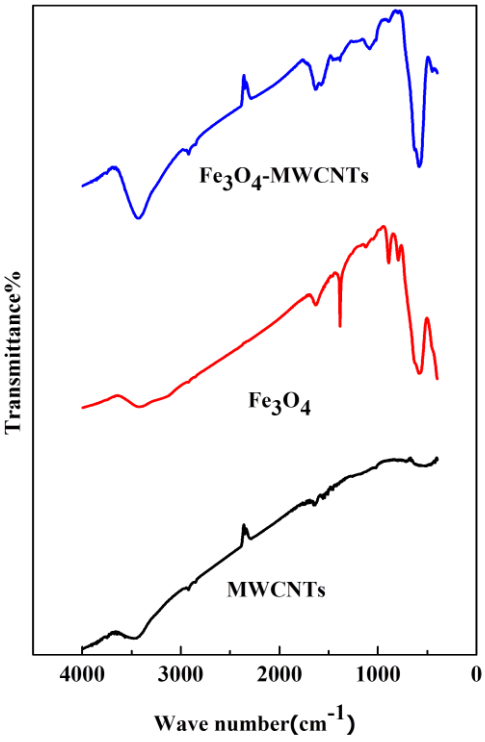

Figure 3. FTIR spectra of pure MWCNTs, Fe_3O_4 and Fe_3O_4–MWCNTs

Table1: Textural property of Fe_3O_4 and Fe_3O_4–MWCNTs samples

Sample	Mean specific surface area $S_{BET}(m^2.g^{-1})$	Mean Total pore volume $V_{Total}(cm^3.g^{-1})$	Mean pore size (nm)
Fe_3O_4	90.026	0.241	13.171
Fe_3O_4–MWCNTs	113.264	0.273	11.195

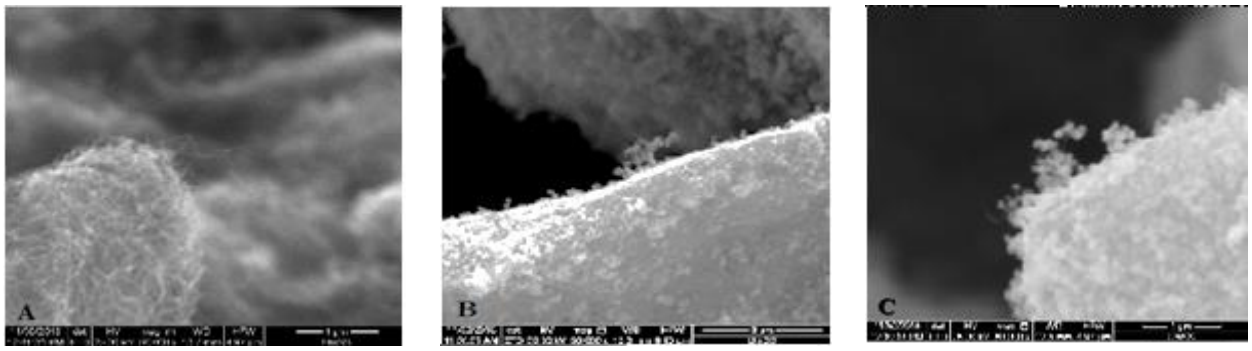

Figure 5. SEM images: (A) MWCNTs, (B) Fe_3O_4 and (C) Fe_3O_4–MWCNTs nanocomposite

3.2. Effect of initial pH

The optimization of pH is very required because it can control both the surface charge of the adsorbent and adsorbate [25]. In this part of study, the effect of initial pH of solution onto the adsorption of BCP was investigated; 20 mg of Fe_3O_4–MWCNTs was added to dye solution (200 mL, 10 mg.L^{-1}) at room temperature and different pH ranging from 5 to 11. (fig.6) shows a slight increase of adsorption capacity in acidic medium until pH = 8 as an optimum value followed by a careless decreasing at pH = 11. The zeta potentials of the adsorbent particles were previously discussed; OH and COOH groups were introduced onto the surface of Fe_3O_4–MWCNTs after the chemical treatment by nitric acid. This leads to the protonation of nanocomposite surface where a positive charge can be dominated in acidic medium [15]. The pH value correlates to Zeta potential of composite Fe_3O_4–MWCNTs was estimated to 6.6 as seen in (fig.6 inset). After this value the negative charges dominated the adsorbent surface in alkaline medium [26]. The Bromocresol purple characterized by acid dissociation constant pK_a equal to 6.3 [11]. Thus the dye molecules are negatively charged in acidic medium and positively charged in basic medium [27, 6]. Hence, a favorable electrostatic attraction occurred between the Fe_3O_4–MWCNTs surface and BCP molecules at all the pH range. Therefore, we can consider the effect of initial pH neglected and carry out the rest of experiments at free pH which was close to 6.

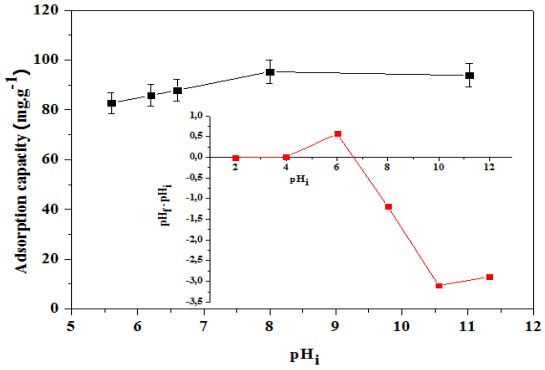

Figure 6. Effect of pH on the adsorption of BCP onto composite (m=20 mg of Fe_3O_4–MWCNTs; 200 mL and 10 mg.L^{-1} of BCP; at room temperature). (Inset) Zeta potential of Fe_3O_4–MWCNTs

3.3. Kinetic study

The interest of this study is to determine the contact time necessary to reach the adsorption equilibrium of BCP dye onto the Fe_3O_4–MWCNTs. As shown in (fig.7), the graph of adsorption capacity Q_t as function of time depicts the adsorption mechanisms as follow, rapid increase of Q_t at the initial stage (20 minutes). After that, a slow adsorption took place (from 20 to 80 minutes); in the last phase (from 80 to 120 minutes) the equilibrium achieved wherein a plateau was observed. As a result, the maximum adsorption capacity and equilibrium time were estimated to be about 90.28 mg.g^{-1} and 80 minutes, respectively. The kinetic models provide us by information about adsorption mechanism and the mode of solute transfer from the liquid phase to the solid phase [28]. For this purpose, the literature reported a number of models such as the Lagergren model or pseudo-first-order model (PFO) [29], the Blanchard model or pseudo-second order kinetic model (PSO) [30] and Weber and Morris model or intraparticle diffusion model [31]. The nonlinear plots of data regression of PFO and PSO were represented in order to determine kinetics using the following expressions in succession [2]:

$$\frac{dq}{dt} = k_1(Q_e - Q_t) \quad (3)$$

$$\frac{dq}{dt} = k_2(Q_e - Q_t)^2 \quad (4)$$

Where k_1 and k_2 are the rate constants for pseudo first and second order kinetics (min^{-1}); Q_t: amount adsorbed at time t (mg. g^{-1}); Q_e: amount adsorbed at equilibrium (mg.g^{-1}) and t: time (min). The equation of intraparticle diffusion model allows the determination of the diffusion rate in pores using the following equation [32]:

$$Q_t = k_d t^{\frac{1}{2}} + C_d \quad (5)$$

k_d (mg.g^{-1}.$min^{-1/2}$) : is the intraparticle diffusion rate constant and C_d(mg.g^{-1}): is the intercept. According to the data summarized in (Table 2), the pseudo second-order is favorable in this adsorption attributed to both of the correlation coefficient and adsorption capacity Q_e. (fig.8) screened that the curve was not linear over the whole time range, it is indicated that not only one process affected the adsorption. As seen from plot pattern there is two stages, the first one is characterized by rapid increase of Q_t at the initial process stage due to the adsorption of dye molecules on the external surface of adsorbent. A slow adsorption

took place referred to the second phase attributed to a slow diffusing of BCP particles into porous structure of nanocomposite because the external sites were occupied very quickly in the first stage.

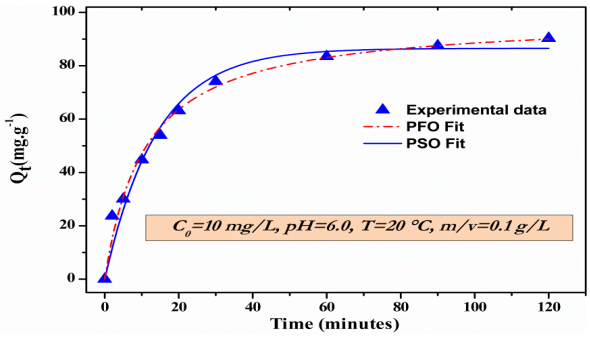

Figure 7. Adsorption kinetic of BCP using Fe_3O_4–MWCNTs

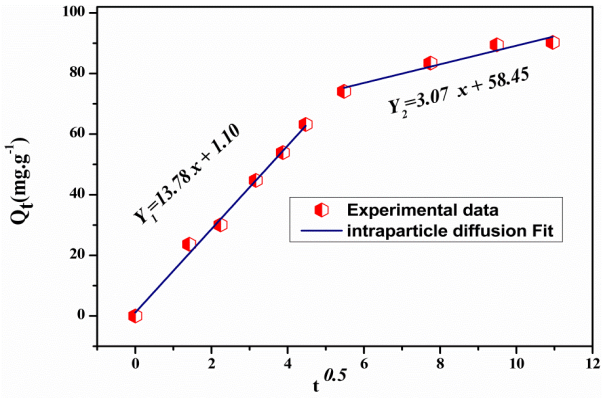

Figure 8. Intra-particle diffusion plot for BCP dye adsorption onto Fe_3O_4–MWCNTs adsorbent

Table 2: Kinetic parameters of PFO, PSO and intraparticle diffusion models.

Kinetic model	$q_{e(exp)}$ (mg.g^{-1})	$q_{e(cal)}$ (mg.g^{-1})	k_1 (L.min^{-1})	R^2	S.E
PFO model	90.28	86.53	0.071	0.972	2.94
PSO model	$q_{e(exp)}$ (mg.g^{-1})	$q_{e(cal)}$ (mg.g^{-1})	k_2 (g.min	R^2	S.E
	90.28	91.12	0.009	0.988	2.91
Intraparticle diffusion model	First step	K_{ip1} (mg.g^{-1}.min$^{-1/2}$)	C_1(mg.g^{-1})	R_1^2	S.E
		13.78	1.10	0.993	1.52
	Second step	K_{ip2} (mg.g^{-1}.min$^{-1/2}$)	C_2(mg.g^{-1})	R_2^2	S.E
		3.07	58.45	0.913	4.66

To conclude, the significant deviation of the line revealed that intra-particle diffusion was not the only rate limiting stage for this process [33].

3.4. Adsorption isotherm models

The modeling of experimental isotherm plays a critical role to understand the sorption process. The isotherm of BCP dye adsorption material was obtained by varying the initial concentration of BCP (from 5 to 50 mg.L^{-1}) at 293±1K. The plot of $Q_e = f(C_e)$ at equilibrium presents the isotherm of BCP adsorption onto Fe_3O_4–MWCNTs which corresponds to isotherm type I according to the Brunauer classification [34]. Among the most used theoretical models, the equilibrium data were fitted to the Langmuir, Freundlich and Dubinin-Radushkevich equations. The Langmuir model suggests that the adsorption takes place on a homogeneous phase, the nonlinear form of Langmuir equation is given by [35]:

$$Q_e = \frac{Q^0_{max}.k_L.C_e}{1+k_L.C_e} \quad (6)$$

Where Q^0_{max} (mg.g^{-1}) represents the maximum monolayer adsorption capacity; k_L(L.mg^{-1}) is the Langmuir constant. The favorability of adsorption can be confirmed using the dimensionless parameter, which is defined as

$$R_L = \frac{1}{1+K_L.C_0} \quad (7)$$

The value of R_L indicates that the type of isotherm can be irreversible if (R_L = 0), unfavorable if (R_L>1), linear if (R_L=1) and favorable while (0<R_L<1) [36].

The Freundlich model assumes that the multilayer adsorption takes place on a heterogeneous surface of adsorbent. This model is given as follows [37]:

$$Q_e = k_F.C_e^n \quad (8)$$

Where k_F is the Freundlich constant associated with adsorption capacity, n indicates the adsorption intensity.

The Dubinin-Radushkevich model is applied to evaluate the free adsorption energy that determines the nature of interactions adsorbent-adsorbate. The nonlinear equation of D-R model is outlined as follows [38]:

$$Q_e = Q_{DR}e^{-k_{DR}.\varepsilon^2} \quad (9)$$

Where Q_{DR} (mg.g^{-1}) is the maximum adsorption capacity; k_{DR}(mol^2.kJ^{-2})constant related to the sorption energy. ε is the Polanyi potential given by:

$$\varepsilon = RT\ln(1+\frac{1}{c_e}) \quad (10)$$

Where R is the gas constant (8.314 J.mol^{-1}.K^{-1}). The mean sorption energy E can be calculated using the following equation:

$$E = \frac{1}{\sqrt{2k_{DR}}} \quad (11)$$

The nature of sorption could be discussed according to the E value; if the magnitude of E is between 8 and 16 kJ.mol^{-1}, the adsorption process is occurred by ion exchange, while the values of E<8 kJ.mol^{-1} reveal the physical nature of interactions [39]. As shown in (fig.9), the data of aforementioned isotherms were plotted using nonlinear forms. According to the outcomes summarized in

(Table.3), the Langmuir model was selected as an optimum adsorption isotherm due to its highest correlation value corresponding to R^2=0.998; the prepared nanocomposite exhibited a high maximum adsorption capacity Q^0_{max}(mg.g^{-1}) estimated to be about 296.52 mg.g^{-1}. In addition, the mean adsorption energy E was found to be about 2.06 kJ.mol^{-1}; it demonstrates the physical nature of dye adsorption onto Fe_3O_4–MWCNTs.

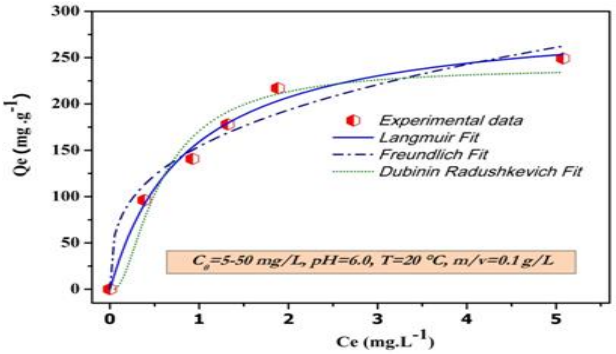

Figure 9. Isotherm models of BCP adsorption onto Fe_3O_4–MWCNTs adsorbent

3.5. *Thermodynamic study*

The thermodynamic study was carried out to estimate standard Gibbs free energy change (ΔG^0), standard enthalpy change (ΔH^0), and standard entropy change (ΔS^0). The different energies can be related with each other by equation (13) as follows [2]:

$$\Delta G^0 = -RTLnK_e \quad (12)$$

$$\Delta G^0 = \Delta H^0 - T\Delta S^0 \quad (13)$$

$$K_e = \frac{Q_e}{C_e} \quad (14)$$

To find the magnitudes of aforementioned energies, the Van'tHoff equation (15) was plotted (fig.10):

$$LnK_e = -\frac{\Delta H^0}{RT} + \frac{\Delta S^0}{R} \quad (15)$$

Where R is the universal gas constant, Q_e is the adsorption capacity at the equilibrium thermodynamic (mg.g^{-1}),C_e is the concentration at the equilibrium, T is the temperature (K), and K_e is the equilibrium thermodynamic constant [40]. (Table.4) shows that exothermic nature of the adsorption phenomena was confirmed by negative value of standard enthalpy change ΔH^0, besides the value of that parameter can give an idea about the type of interactions between adsorbate and adsorbent, therefore 15.45kJ.mol^{-1} is lower than 20 kJ.mol^{-1} indicates that van der Waals interactions occurred between BCP molecules and Fe_3O_4–MWCNTs particles, so then the physisorption type took place in this case. The negative values of standard Gibbs free energy change ΔG^0 show that the adsorption process was favorable, spontaneous and enthalpy controlled, where the negative value of ΔS^0 exhibites the decrease of randomness at the interface solid-liquid when the adsorption occurred [2,41].

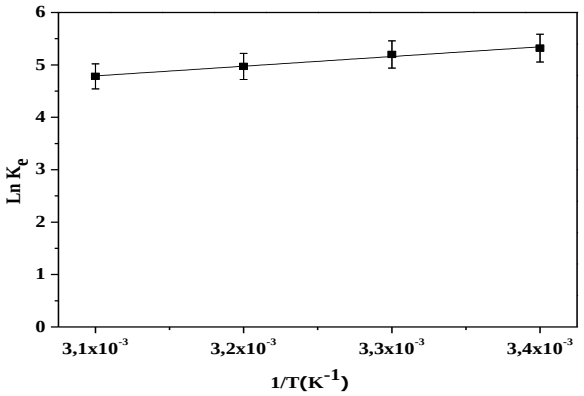

Figure 10. Effect of temperature on the equilibrium thermodynamic constant

Table 3: Isotherm constant parameters for the BCP adsorption onto Fe_3O_4–MWCNTs adsorbent

Models	Parameter				
Langmuir	Q^0_{max}(mg.g^{-1}) 296.52	k_L(L.mg^{-1}) 1.160	R^2 0.988	SE 16.3	R_L 0.079
Freundlich	k_F(mg.g^{-1}) 154.22	n 0.327	R^2 0.957	SE 9.55	-
Dubinin–Radushkevich	Q_{max}(mg.g^{-1}) 239.47	k_{DR}(mol^2.K^{-1}J^{-2}) 1.18×10^{-7}	R^2 0.956	SE 14.51	E(kJ.mol^{-1}) 2.06

Table 4: Thermodynamic parameters of BCP adsorption onto Fe_3O_4–MWCNTs adsorbent

ΔG^0 (kJ.mol^{-1})				ΔH^0(kJ.mol^{-1})	ΔS^0(J.mol^{-1}.K^{-1})	R^2
293 K	303 K	313 K	323 K	-15.45	-8.09	0.981
-13.08	-13.00	-12.66	-12,84			

4. Conclusion

Efficiently, a small amount of nanocomposite Fe_3O_4–MWCNTs exhibited a high adsorption capacity of BCP from aqueous solution 296.52 $mg.g^{-1}$; without high energy or complicated devices. This study highlights the modification of MWCNTs by magnetite which offers a simple separation and low cost adsorbent compared with pristine multi-walled carbon nanotubes. Kinetic study indicated that the pseudo second order fitted well the process. Meanwhile, the Langmuir isotherm best suited the experimental data. Results suggest that the adsorbent can have a potential application in industry.

Acknowledgments

The authors thank Pr. Plinio Innocenzi, Dr. Luca Malfatti, Róbert Ludmerczki (Materials Science and Nanotechnology Laboratory, Sassari, Italy) for their technical supports.

References

[1] M. Larakeb, L. Youcef, S. Achour, J. New Technol. Mater. 6 (2016) 19.
[2] A. Bonilla-Petriciolet, D. I. Mendoza-Castillo, H. E. Reynel-Ávila, Eds., Adsorption Processes for Water Treatment and Purification, Springer International Publishing, Cham, 2017.
[3] M. A. Al-Ghouti, M. A. M. Khraisheh, S. J. Allen and M. N. Ahmad, Journal of Environmental Management. 69 (2003) 229.
[4] P. B. Biru, D. R. Oren and Y. Diquarternasi, Malaysian Journal of Analytical Sciences 13 (2009) 185.
[5] V. Hernández-Montoya, M. A. Pérez-Cruz, D. I. Mendoza-Castillo, M. R. Moreno-Virgen and A. Bonilla-Petriciolet , Journal of Environmental Management. **116** (2013) 213.
[6] L. Aljerf, Journal of Environmental Management. 225 (2018) 120.
[7] R. Shrivastava, V. Christian and B. R. M. Vyas, Enzyme and Microbial Technology. 36 (2005) 333.
[8] L. C. Morais, O. M. Freitas, E. P. Gonçalves, L. T. Vasconcelos and C. G. González Beça, Water Research. 5 (1999) 979.
[9] M. C. Pereira, L. C. A. Oliveira and E. Murad, Clay miner. 47 (2012) 285.
[10] S. G. de Moraes, R. S. Freire and N. Dura, Chemosphere . 40 (2000) 369.
[11] F. El-dars, MSE, Ibrahim, H.M., Farag, Int. J. Sci. Eng. Res. 6 (2015) 6188.
[12] I. Bousnoubra, K. Djebbar, A. Abdessemed and T. Sehili, Desalination and Water Treatment, (2016) 1.
[13] S. Mallakpour, V. Behranvand, F. Mallakpour, Carbohydrate Polymers. 224 (2019) 115.
[14] H. Gao, S. Zhao, X. Cheng, X. Wang and L. Zheng, Chemical Engineering Journal. 223 (2013) 84.
[15] N. Dalali, M. Habibizadeh, K. Rostamizadeh and S. Nakisa, Asia-Pac. J. Chem. Eng. (2014).
[16] W. Yan, G. Lian, S. Jing et al, Chemical physics letters. 432 (2006) 205.
[17] R. M. Lago, S. C. Tsang, K. L. Lu, Y. K. Chen and M. L. H. Green, J. Chem. Soc., Chem. Commun. (1995) 1355.
[18] P. L. Hariani, M. Faizal, R. Ridwan, M. Marsi and D. Setiabudidaya, IJESD (2013) 336.
[19] N. Fayoud, S. A. Younssi, S. Tahiri and A. Albizane, J. Mater. Environ. Sci. *6* (2015) 12.
[20] V. Cleveland, J.-P. Bingham and E. Kan, Separation and Purification Technology. 133 (2014) 388.
[21] L. Houcine, L. Sonia, R. Schneider and T. B. Chaabane, Chemistry Africa. 1 (2018) 37.
[22] W.Yan, H.Bing, H. Xiaoyang, Procedia Engineering. 27 (2012) 632.
[23] X. Hu, B. Liu, Y. Deng, H. Chen, S. Luo, C. Sun, P. Yang and S. Yang, Applied Catalysis B: Environmental. 107 (2011) 274.
[24] M. H. Razali, A. Ahmad, M. A. Azaman and K. A. M. Amin. Inter J of app chem. 12(2016)273.
[25] A. T. Vo, V. P. Nguyen, A. Ouakouak, B. T. Nieva, A., Doma, H. N. Tran, H. P. Chao, Water. 11(2019) 1164.
[26] X. Bai, Liu, Y.L. Yu, Z. Hua, Scientific reports. *6* (2016) 32845.
[27] H. Tavakkoli, A. Ghaemi, M. Mostofizadeh, Int. J. Sci. Resin Knowledge. 2 (2014) 340.
[28] Y. Ho, Journal of Hazardous Materials. 136 (2006) 681.
[29] A. S. Özcan, B. Erdem, A. Özcan, Colloids and Surfaces A: Physicochemical and Engineering Aspects. 226 (2005) 73.
[30] Y. S. Ho and G. McKay, Wat Res. **33** (1999) 578.
[31] W. J. Weber and J. C. Morris, Journal of the Sanitary Engineering Division . 89 (1963) 31.
[32] N. Rouahna, D. Barkat, A. Ouakouak and E. Srasra, Journal of Environmental Chemical Engineering. 6 (2018) 1226.
[33] L.M.SUN and F. Meunier, Techniques de l'ingénieur Génie des procédés. 2 (2003) 2730.
[34] I. Langmuir, J. Am. Chem. Soc. 40(1918)1361.
[35] K. R. Hall, L. C. Eagleton, A. Acrivos and T. Vermeulen, Industrial & Engineering Chemistry Fundamentals. 5(1966)212.
[36] O. Hamdaoui and E. Naffrechoux, Journal of Hazardous Materials. 147 (2007) 381.
[37] H. Freundlich, Zeitschrift für Physikalische Chemie. 57 (1907) 385.
[38] K. O. Adebowale, B. I. Olu-Owolabi and E. C. Chigbundu, JEAS. 04 (2014) 89.
[39] A. S. Özcan, B. Erdem and A. Özcan, Colloids and Surfaces A: Physicochemical and Engineering Aspects. 266 (2005) 73.
[40] A. S. Özcan and A. Özcan, Journal of Colloid and Interface Science. 276 (2004) 39.
[41] G. Crini and P.-M. Badot, Progress in Polymer Science. 33 (2008) 399.